



Use of alkali activated high-calcium fly ash binder for kaolin clay soil stabilisation: Physicochemical evolution

Elodie Coudert, Michael Paris, Dimitri Deneele, Giacomo Russo, Alessandro Tarantino

► To cite this version:

Elodie Coudert, Michael Paris, Dimitri Deneele, Giacomo Russo, Alessandro Tarantino. Use of alkali activated high-calcium fly ash binder for kaolin clay soil stabilisation: Physicochemical evolution. Construction and Building Materials, 2019, 201, 14p. 10.1016/j.conbuildmat.2018.12.188 . hal-01976909

HAL Id: hal-01976909

<https://hal.science/hal-01976909v1>

Submitted on 21 Oct 2021

HAL is a multi-disciplinary open access archive for the deposit and dissemination of scientific research documents, whether they are published or not. The documents may come from teaching and research institutions in France or abroad, or from public or private research centers.

L'archive ouverte pluridisciplinaire **HAL**, est destinée au dépôt et à la diffusion de documents scientifiques de niveau recherche, publiés ou non, émanant des établissements d'enseignement et de recherche français ou étrangers, des laboratoires publics ou privés.



Distributed under a Creative Commons Attribution - NonCommercial 4.0 International License

Use of alkali activated high-calcium fly ash binder for kaolin clay soil stabilisation:

Physicochemical evolution

Elodie Coudert^{a,b,c}, Michael Paris^a, Dimitri Deneele^{a,d*}, Giacomo Russo^b, Alessandro Tarantino^c

^a Institut des Matériaux Jean Rouxel (IMN), Université de Nantes, CNRS, 2 rue de la Houssinière, BP 32229, 44322 Nantes Cedex 3, France

^b Department of Civil and Mechanical Engineering, University of Cassino and Southern Lazio, Via Gaetano di Biasio, 43, 03043 Cassino, FR, Italy

^c Department of Civil and Environmental Engineering, University of Strathclyde, 75 Montrose Street, Glasgow, Scotland, G1 1XJ, United Kingdom

^d IFSTTAR, GERS, EE, F-44344 Bouguenais, France.

*Corresponding author

Phone : + 33 2 40 84 58 02

Fax: + 33 2 40 58 57 77

E-mail: Dimitri.Deneele@ifsttar.fr

Abstract

This study addresses the use of alkali activated high-calcium fly ash-based binder to improve engineering characteristics of soft clay-rich soils as an alternative to common stabilisers. The physico-chemical reaction sequence has been investigated by considering the binder alone and the binder mixed with kaolin. An insight into the reactivity evidenced that calcium-containing phases derived from high-calcium fly ash represent the reactive phases and, hence, pozzolanic activity is the dominant process. New compounds are formed, thenardite Na_2SO_4 and an amorphous silicate consisting of

25 chains combined with calcium probably incorporating three-dimensional four-fold
26 aluminium environments.

27 **Keywords**

28 Soil stabilisation; Alkali activated material; Kaolin; High-calcium fly ash

29

30 **1. Introduction**

31 Soft clay-rich soils are frequently encountered in construction sites. Their poor
32 mechanical performance represents a critical issue in engineering projects. These soils
33 cannot be directly used as earthfill materials and may cause excessive settlements of
34 foundation structures. To improve their engineering characteristics chemical
35 stabilisation involving the addition of a binder to the soil has been widely practiced. The
36 commonly used stabilisers are Ordinary Portland Cement and lime whose stabilisation
37 mechanisms have been widely reported [1-7]. Nevertheless, a major issue with those
38 conventional stabilisers is a very significant environmental penalty due to high carbon
39 dioxide emissions and energy intensive processes.

40 In the low carbon agenda, the development of novel technologies that are both cost- and
41 carbon-efficient is of prime importance, particularly in the construction sector for which
42 cement production contributes to at least 5–8% of global carbon dioxide emissions [8].
43 As an alternative, industrial by-products such as high-calcium fly ash, rice husk ash, and
44 silica fume have been successfully mixed as cementing additives to soft soils resulting
45 in environmental and economic benefits [9-15].

46 Another alternative gaining attention is the use of Alkali Activated Materials as a viable
47 sustainable binder whose often-claimed advantage is a much lower CO₂ emission
48 process compared to traditional Portland cement. Works on alkali activated soils are
49 recent and aim to stabilise different types of soil from clayey soil [16-17], sandy clay
50 [18], Lateritic soils [19] marl, marlstone [20], silty sand [21], road aggregates [22] to
51 mixed soil synthesised in laboratory [23-24]. The overall work shows the potential of
52 alkaline activation for soil improvement, and this for different designed applications i.e.
53 in deep soft soil [18], at shallow depth [24] or in rammed earth construction [25].

54 Alkali Activated Materials are defined as any binder system derived by the reaction of
55 an alkali metal source (usually alkali hydroxide and alkali silicate solutions) with a solid
56 aluminosilicate powder (commonly metakaolin, fly ash, blast furnace slag or natural
57 pozzolan) [26-27]. It gives a hardened material at room temperature with mechanical
58 properties potentially suitable for Portland cement replacement.

59 The type of aluminosilicate material needed in the alkali activation process varies as
60 well. In fact, most of the studies were conducted on the use of fly ash [16-18; 20-21; 23-
61 25; 28-29]. Nevertheless, Zhang et al. [24] also examined the feasibility of metakaolin
62 based alkali activated soil, and some other studies established on slag based alkali
63 activated soil are as well existing [16, 17, 23].

64 As stabilisation using alkaline activation is a recent research area, studies about the
65 understanding of the physicochemical reactivity of such systems have received little
66 attention so far [17] . Yet, the molecular structure and the chemical composition of the
67 alkali activated binders is essential to properly assess the resulting strength and
68 durability of the final material.

69 This work focuses on the use of calcium-rich high-calcium fly ash from coal
70 combustion activated by sodium-based alkaline solution as a binder for clay kaolin
71 stabilisation. High-calcium fly ash was selected in the context of resource-saving being
72 an industrial waste. Kaolin was selected as a model soil to represent a wide class of
73 clays encountered in engineering projects.

74 The study was designed in three stages. An initial stage consisted in the investigation of
75 the reactivity of the alkali activated high-calcium fly ash binder by itself, including (i)
76 which phases are present and which phases are accessible during alkaline activation, (ii)
77 which compounds are subsequently formed, and (iii) reactivity timescale. A second

78 stage focused on the interaction of the high-calcium fly ash-based binder with the kaolin
79 clay to understand how the presence of kaolin modifies the reactivity of the system.
80 Kaolinite is generally unreactive to alkali attack at ambient temperature. However, the
81 addition of clay may affect chemical reactions as occurs in clay-cement mix [30].
82 Finally, the physicochemical evolution occurring in the alkali activated high-calcium fly
83 ash is compared with one occurring in the same kaolin stabilised by i) lime or ii) a mix
84 of lime and the same high-calcium fly ash used in this experimental programme. This is
85 aimed at assessing the potential benefit of high-calcium fly ash-based binder compared
86 to the more traditional lime.

87

2. Material and methods

2.1 Materials

A Polish high-calcium fly ash derived from hard coal and coal slime combustion in fluidised bed boiler was used. Its chemical analysis is given in Table 1, and consists primarily of SiO₂, Al₂O₃ and CaO. The high-calcium fly ash contains, approximately, 52% of particles sized lower than 45 µm and 41% lower than 10 µm.

Speswhite kaolin provided by Imerys Minerals UK, and whose chemical composition is given in Table 1 was used. It is mainly constituted of kaolinite (95%) and secondarily of muscovite (4%) [3]. The kaolin contains, approximately, 100 % of particles sized lower than 10 µm and 80 % lower than 2 µm.

A unique alkaline solution was used: a sodium silicate with a mass ratio SiO₂/Na₂O of 1.7 and a dry mass percentage of 44%; supplied by Woellner group and named GEOSIL 34417.

Table 1

Chemical composition (wt. %) of raw fly ash and kaolin.

	SiO ₂	Al ₂ O ₃	Fe ₂ O ₃	CaO	CaO _{free} ^a	MgO	SO ₃	Na ₂ O	K ₂ O	H ₂ O	L.o.I.
Fly ash	39.4	19.8	7.4	18.6	5.2	1.8	4.1	2.0	1.8	0.0	1.7 ^b
Kaolin	49.2	34.5	1.2	0.0	0.0	0.2	0.0	0.1	1.7	13.1	12.0 ^c

^a Free calcium oxide content, ^b from [3], ^c from [33]

2.2 Sample preparation

Sample preparation consisted in (i) mix of liquid sources ie. silicate and water (ii) mix of aluminosilicate powders ie. high-calcium fly ash and kaolin in the case of soil-source sample (iii) mix of (i) and (ii) previously prepared.

Three types of mixes were studied and named F100, KF50 and KF20. F100 is the high-calcium fly ash based alkali activated binder. It corresponds to a solid phase made of

high-calcium fly ash only, whereas KF50 and KF20 are the alkali activated soils. KF50 corresponding to a solid phase made of 50% of high-calcium fly ash and 50% of kaolin in mass, and KF20 corresponding to a solid phase made of 20% of high-calcium fly ash and 80% of kaolin. List of samples is summarized up in Table 2.

To ensure a good workability, the amount of added water with respect to the solid mass (eg. mass of kaolin and high-calcium fly ash) was fixed to 50% for all the samples. Additionally, the mass ratio of alkaline solution to high-calcium fly ash was fixed to 50% for all the samples, giving the initial molar ratios (considering that kaolin is unreactive): $\text{Si/Al} = 2.0$, $\text{Si/Na} = 3.5$ and $\text{Al/Na} = 1.8$. The Al/Na ratio was not fixed to one because of the presence of calcium ions in high quantity in our system playing a role of charge compensation as well as sodium.

The paste obtained was poured in closed plastic molds and cured at room temperature (20 °C). Samples were finally demoulded and freeze dried at curing times of 1, 3, 7 or 28 days.

Table 2

Samples composition wt. %.

Sample	Fly ash	Kaolin	Water	Alkaline solution
F100	50	0	25	25
KF50	28.6	28.6	28.6	14.3
KF20	12.5	50	31.3	6.3

126
127

2.3 Methods

A variety of characterisation techniques were complementary used to probe the mineralogical, structural and microstructural sample characteristics.

131 X-ray diffractograms of powdered samples were obtained with a Bruker D8 Advance
132 diffractometer, using CuK α radiation generated at 40 mA and 40kV. Specimens were
133 step-scanned from 2 to 60° 2 θ at 0.017° 2 θ steps integrated at the rate of 1s/step.

134 Derivative thermogravimetric curves were obtained on a Netzsch STA 449F3 Jupiter
135 thermal analyser. The samples were heated from 20–1000 °C at a rate of 10 °C/min
136 under argon atmosphere.

137 FTIR spectra were obtained on an FTIR Bruker Vertex 70 spectrometer. Specimens
138 were prepared by mixing 30 mg of sample in 270 mg of KBr. Spectral analysis was
139 performed over the range 4000–400 cm⁻¹ at a resolution of 4 cm⁻¹.

140 Solid-state ²⁹Si NMR spectroscopy was performed using a Bruker Avance III 300 MHz
141 (7 T) spectrometer and 7 mm MAS probe. ²⁹Si MAS spectra were acquired with a single
142 $\pi/2$ pulse excitation of 5.5 μ s and ¹H decoupling. The repetition times were 2 s, 120 s
143 and 30 s for the raw high-calcium fly ash, the raw kaolin and all the activated samples,
144 respectively. For all ²⁹Si spectra, MAS spinning rate was set to 5 kHz. Solid-state ²⁷Al
145 NMR spectroscopy was performed using a Bruker Avance III 500 MHz (11.7 T)
146 spectrometer and 2.5 mm MAS probe. ²⁷Al MAS spectra were acquired with a single
147 pulse excitation of $\pi/12$ pulse of 3.3 μ s and ¹H decoupling. Repetition time was set to 1
148 s and MAS spinning rate to 30 kHz. Spectra were referenced against TMS
149 (tetramethylsilane) for ²⁹Si and an Al(NO₃)₃ aqueous solution for ²⁷Al. Lastly, attention
150 should be drawn to the fact that iron initially present in the high-calcium fly ash renders
151 the interpretation more complex, notably spectra from different mixes cannot be
152 quantitatively compared.

153 Finally, samples were studied by SEM from polished section. Freeze-dried samples
154 were impregnated under a vacuum with an acrylic resin (LR White). The polymerisation

155 of the resin was performed in an oven at 60°C over 48 h. The samples were then
156 polished with diamond powder and coated with carbon before the observation. The
157 observations were done with a HITACHI SU5000 scanning electron microscope
158 equipped with an energy-dispersive X-ray analyser (Quantax microanalyser system
159 composed of X-Flash® SDD detector and the Esprit software). The microscope was
160 operated at an accelerating voltage of 20 kV and working distances of 10 mm.

161 **3. Results and discussion**

162 The first section of results presents the physico-chemical evolution of the binder alone
163 without the addition of kaolin. The second part focuses on the description of the soil
164 source material mixed with binder. To end with, the system investigated in this study is
165 compared with lime-based systems already described in the literature.

166 *3.1 Alkali activated high-calcium fly ash binder*

167 *3.1.1 X-ray diffraction (XRD)*

168 Results obtained by XRD show that the original high-calcium fly ash is constituted of a
169 vitreous phase (hump between 17°2θ and 38°2θ), and crystalline phases which include
170 calcium-containing minerals: anhydrite CaSO₄, calcite CaCO₃ and portlandite Ca(OH)₂,
171 and other minerals: quartz SiO₂, feldspar (K,Na,Ca)(Si,Al)₄O₈, hematite Fe₂O₃ and
172 muscovite (Si₃Al)O₁₀(Al₂)(OH)₂K (Fig. 1).

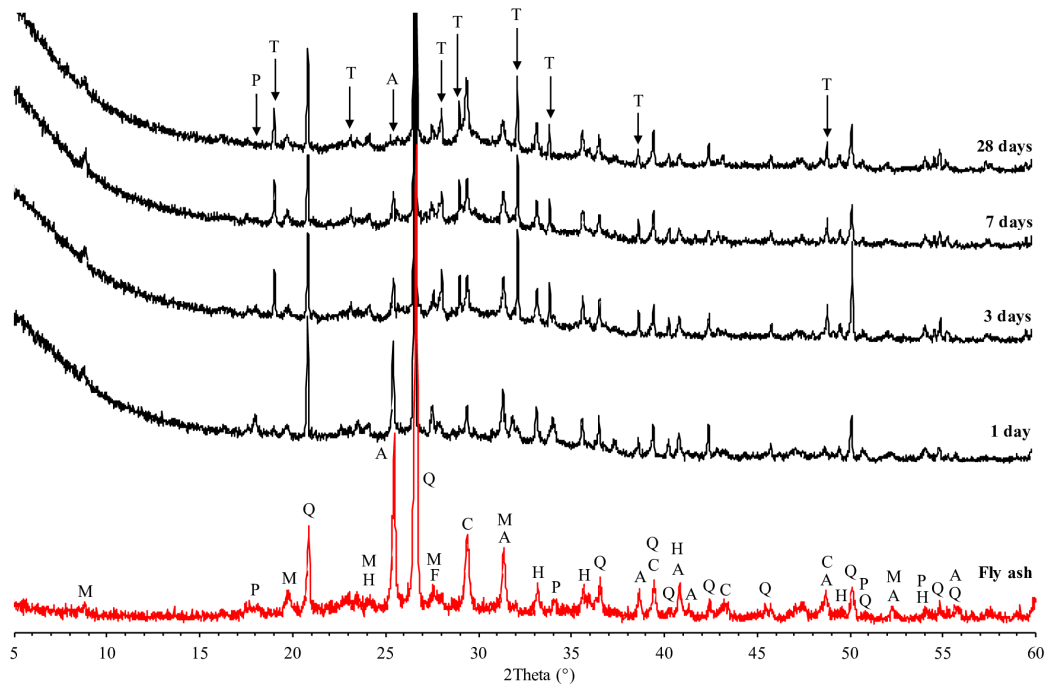


Fig. 1. XRD of raw fly ash and fly ash based alkali activated material F100 as a function of curing time; A=anhydrite; C=calcite; F=feldspar; H=hematite; M=muscovite; P=portlandite; Q=quartz; T=thenardite.

Fig. 1 also shows XRD patterns of the alkali activated high-calcium fly ash as a function of curing time. Regarding the crystalline phases, anhydrite CaSO_4 and portlandite Ca(OH)_2 are consumed as a function of time. In addition, thenardite Na_2SO_4 starts forming at 3 days. Its formation can be explained by the release of sulphate anions from anhydrite dissolution, and its subsequent combination with sodium issued from the alkaline solution.

3.1.2 Derivative thermogravimetric analysis (DTG)

Fig. 2 shows derivative thermogravimetric analyses of the original high-calcium fly ash, and the high-calcium fly ash based alkali activated binder as a function of time. The DTG peaks of the original high-calcium fly ash detected at 385, 605 and 965 °C indicate the decomposition of portlandite Ca(OH)_2 , calcium carbonate CaCO_3 and anhydrite CaSO_4 respectively.

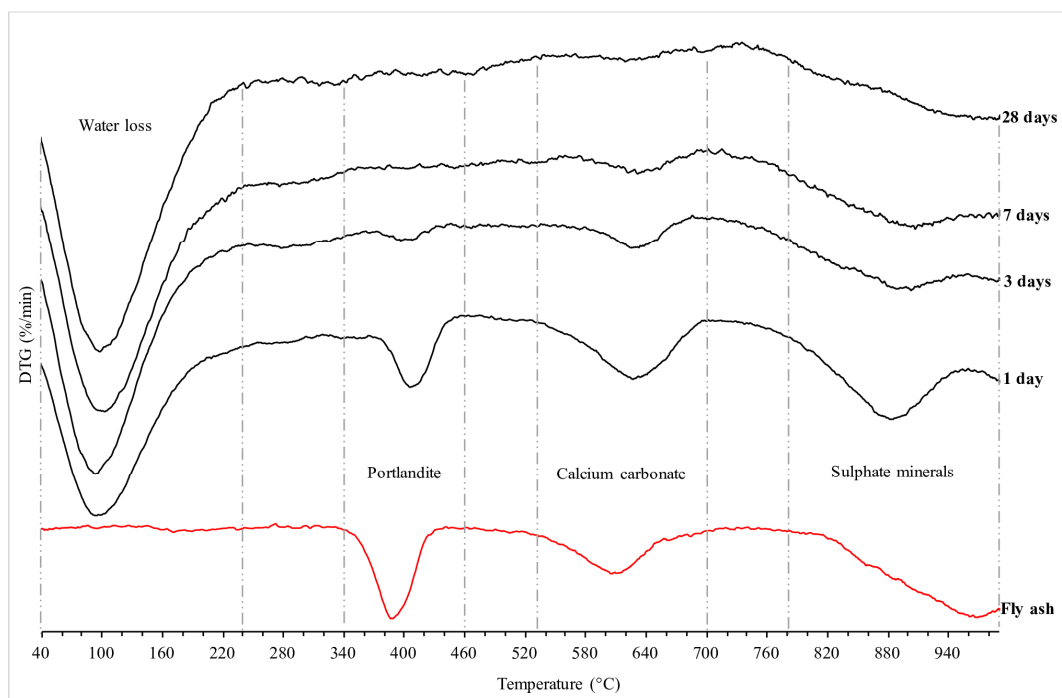


Fig. 2. DTG curves of raw fly ash and fly ash based alkali activated material F100 as a function of curing time.

The relatively low decomposition temperature of anhydrite compare to its theoretical decomposition at 1214°C [31] is ascribed to the fact that anhydrite is found interlinked with other calcium-rich phases by SEM (as illustrated later in section 3.1.4.1).

Regarding the alkali activated high-calcium fly ash, and complementary to XRD, thermogravimetric analyses confirm the consumption of portlandite $\text{Ca}(\text{OH})_2$ over time. DTG curves also show the dissolution of calcium carbonate CaCO_3 with time. Finally, above 780 °C, the observed mass losses of the activated samples reveal the decomposition of sulphate minerals: anhydrite CaSO_4 , thenardite Na_2SO_4 being formed from 3 days as detected earlier by XRD (see 3.1.1), for which theoretical polymorphic transformation occurs at around 900°C [32-33].

3.1.3 Fourier Transform Infrared spectroscopy (FTIR)

Fig. 3A shows FTIR spectra of the original high-calcium fly ash, and the high-calcium fly ash based alkali activated binder as a function of time in the range of CO_3^{2-} stretching vibrations.

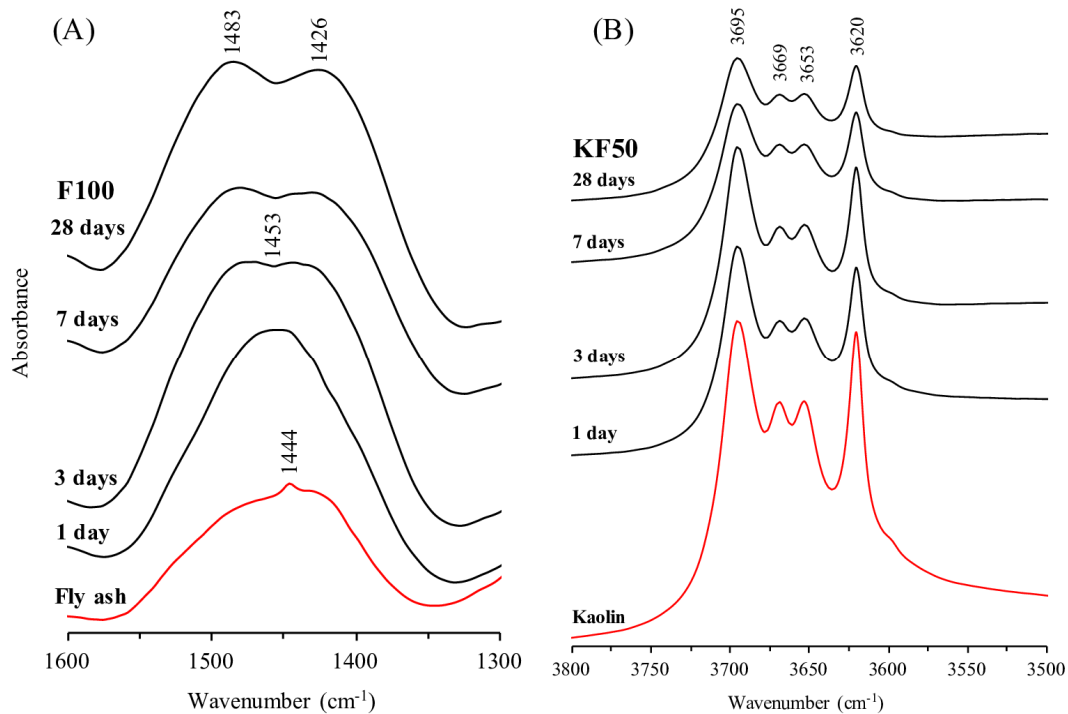


Fig. 3. FTIR of raw fly ash and fly ash based alkali activated material F100 as a function of curing time in the CO_3^{2-} stretching vibrations range (A) and raw kaolin and alkali activated kaolin KF50 as a function of curing time in the OH stretching vibrations range (B).

Different features of the CO_3^{2-} band is observed over time: at 1 day a single band around 1453 cm^{-1} is seen, while at 28 days a doublet positioned at 1426 and 1483 cm^{-1} is observed. Those modifications validate the formation of calcium carbonate during the curing time as observed by DTG.

Finally, Fig. A.1 (see appendices) shows FTIR spectra in the area of sulphate minerals. It confirms the dissolution of calcium sulphate (anhydrite, CaSO_4) along with the subsequent formation of sodium sulphate (thenardite, Na_2SO_4) as previously seen by XRD (see 3.1.1).

216 3.1.4 Scanning Electron Microscopy (SEM)

217 3.1.4.1 Calcium-rich phases

218 Fig. 4 shows SEM observations of the alkali activated high-calcium fly ash at 1 day.

219 More specifically, it focuses on calcium-rich phases previously detected as reactive
220 phases being dissolved following the alkali attack by XRD, TGA and FTIR.

221 Calcium-rich phases are initially present in high-calcium fly ash as nodules of large size
222 from 100 to 250 μm . Besides, it is seen that chemical elements such as calcium, sulphur
223 and silicon are not homogeneously spread within nodules suggesting a varying
224 mineralogy. For instance, in area 2, despite a high content of sulphur indicating a
225 prevalence of anhydrite (CaSO_4), the detected percentage of SO_3 with respect to CaO
226 remains too low to be owed to the presence of anhydrite phases only. It is therefore
227 concluded that the various calcium-containing phases such as anhydrite CaSO_4 , calcite
228 CaCO_3 and portlandite $\text{Ca}(\text{OH})_2$ (previously detected by XRD and DTG in section 3.1.1
229 and 3.1.2) are interlaced within those nodule structures which represent reactive
230 structures under alkaline attack.

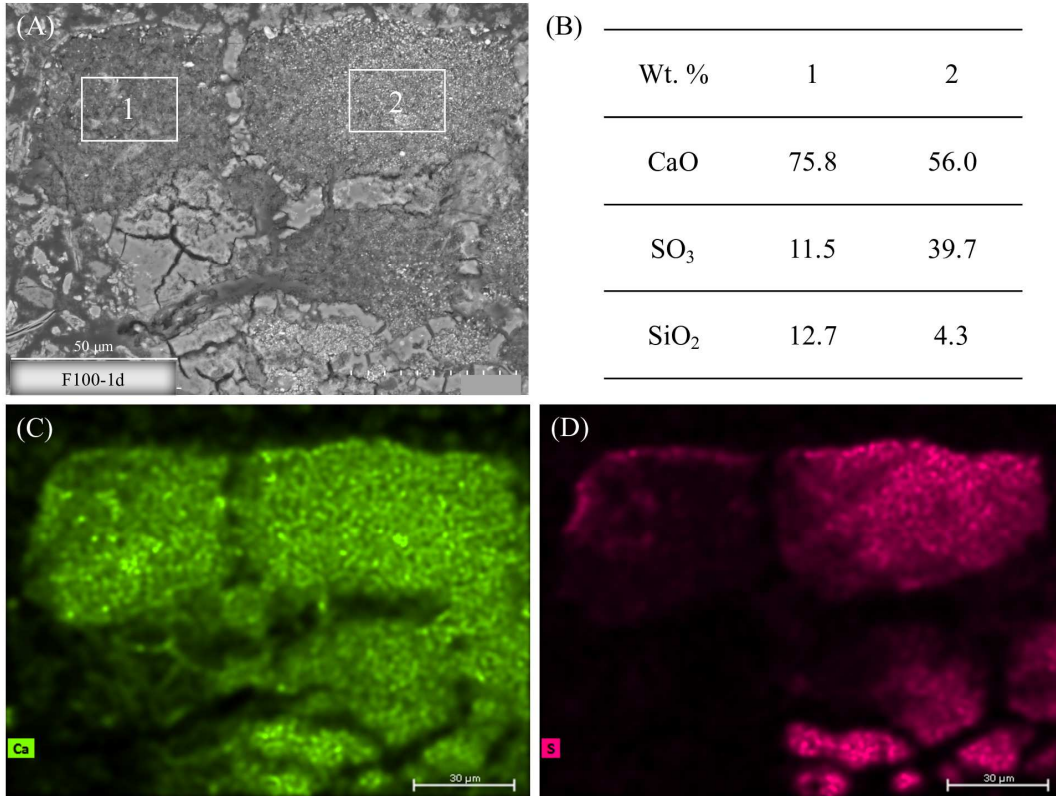


Fig. 4. SEM observations of a calcium-rich nodule from the alkali activated fly ash at 1 day: (A) SEM micrograph, (B) chemical composition (wt. %) of areas 1 and 2, (C) and (D) chemical mappings of calcium and sulphur respectively.

Overall sample

Fig. 5 additionally shows microstructural observations of the alkali activated high-calcium fly ash binder. At 1 day (Fig. 5A), a porous material along with distinct unreacted high-calcium fly ash particles is seen. In contrast, at 28 days (Fig. 5B), a more compact material with less pores is observed evidencing the formation of new compounds. Moreover, at 28 days, several unreacted high-calcium fly ash particles are still observed especially from the vitreous phase i.e. spherical and vesicular particles (see Fig. 5B, C and D).

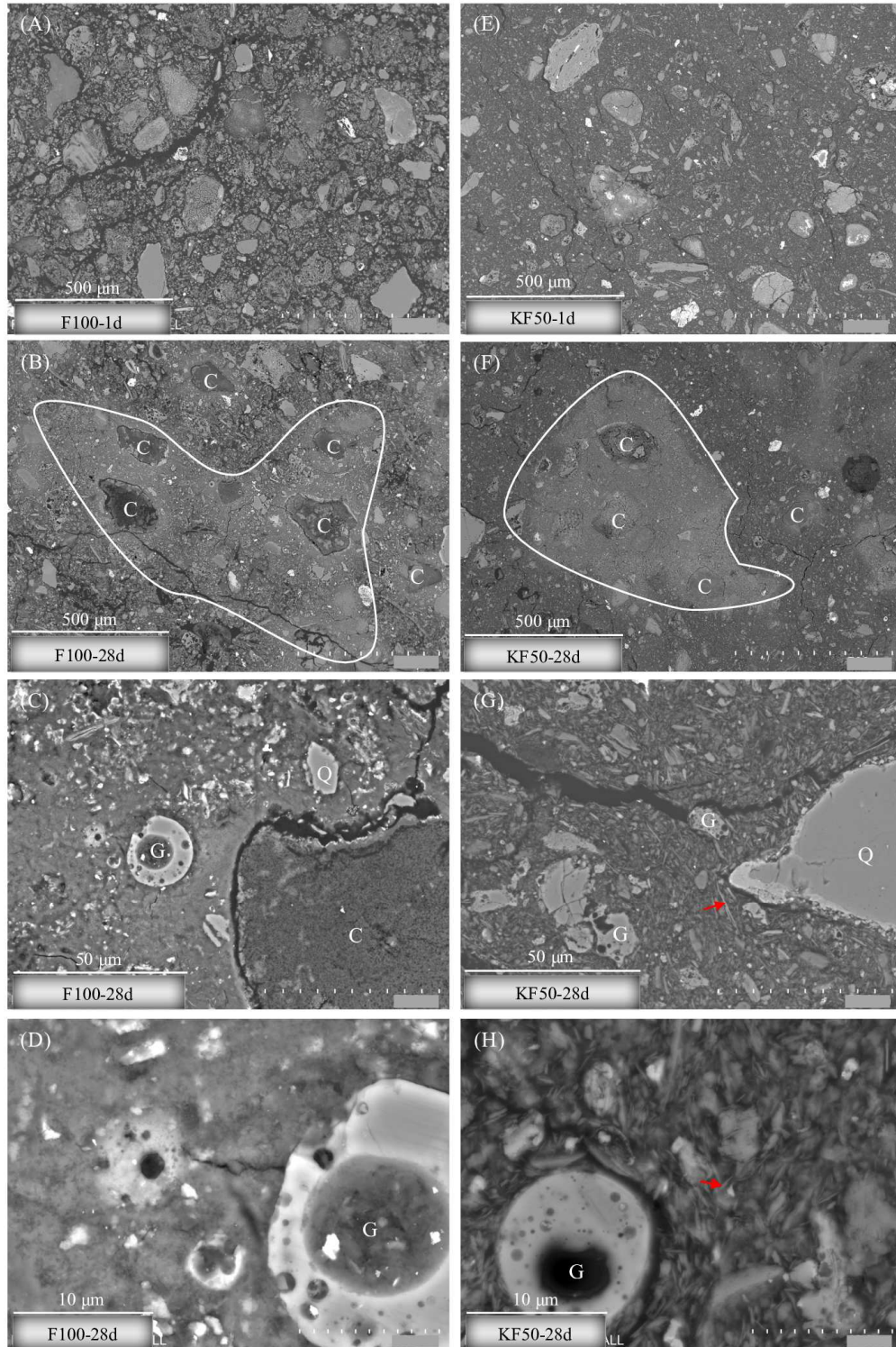


Fig. 5. SEM micrographs of (i) the alkali activated fly ash binder F100 (Column 1) (A) at 1 day and (B), (C) and (D) at 28 days, (ii) the alkali activated kaolin KF50 (Column 2) (E) at 1 day and (F), (G) and (H) at 28 days; C=calcium nodules; G=glass; Q=quartz.

Additional chemical analyses revealed that changes in microstructure are more significant around calcium-rich particles which were previously detected as the main reactive part of the raw high-calcium fly ash.

As a matter of fact, SEM micrographs show zones of higher density appearing brighter around calcium-rich nodules (see encircled area in Fig. 5B).

Table 3 gives an average chemical composition of the denser reactive areas. Notably, it indicates a ratio of sodium to sulphur around 2 matching with that of precipitated thenardite whose formula is Na_2SO_4 , and implying that most of the sodium from the alkaline solution is taken up to form thenardite.

Table 3

Average elemental composition (wt. %) of F100 and KF50 denser areas at 28 days.

	Si	Ca	Al	Na	S	K	Fe	Mg	O
F100-28d	22.1	19.2	7.0	3.7	1.7	1.2	0.8	0.5	43.8
KF50-28d	24.1	14.5	8.8	3.1	1.6	1.6	0.7	0.3	45.3

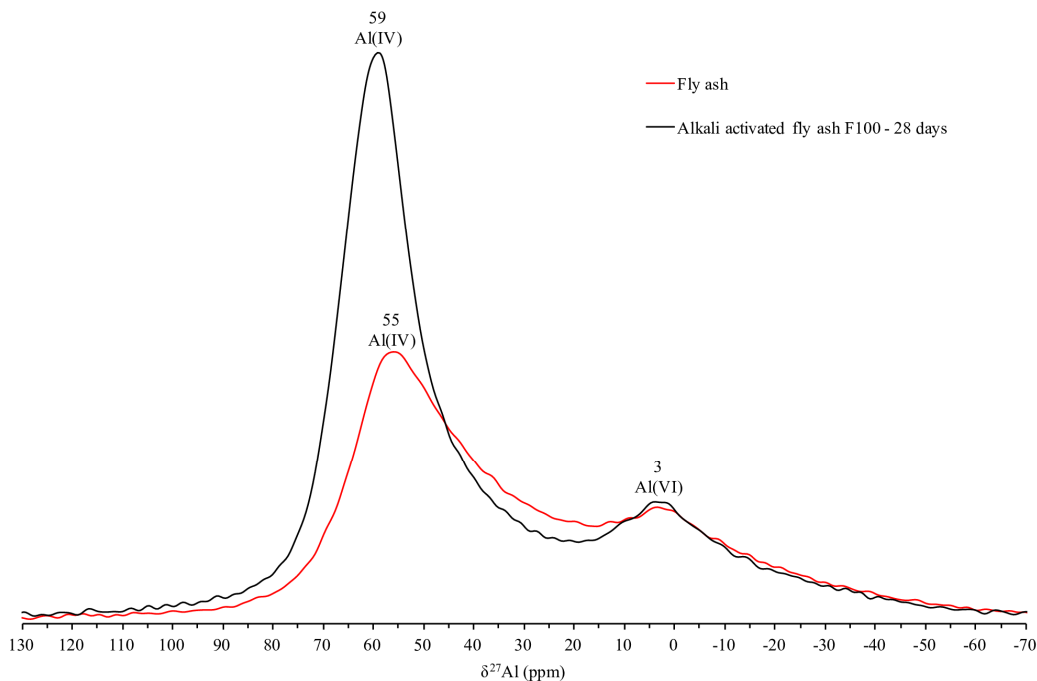
Furthermore, Table 3 indicates that the massive reactive area is primarily composed of silicon and calcium. Supposing that the new compounds are mainly located in those denser areas, these results suggest that apart from thenardite the new compounds are enriched in silicon and calcium.

3.1.5 Nuclear Magnetic Resonance (NMR)

Nuclear Magnetic Resonance was finally used to follow amorphous phases and precise the structure of the new compounds formed in our investigated system.

Fig. 6 shows ^{27}Al MAS-NMR spectrum of the original high-calcium fly ash as well as the spectrum belonging to the alkali activated high-calcium fly ash at 28 days. ^{27}Al NMR spectrum of the original high-calcium fly ash displays two resonances whose

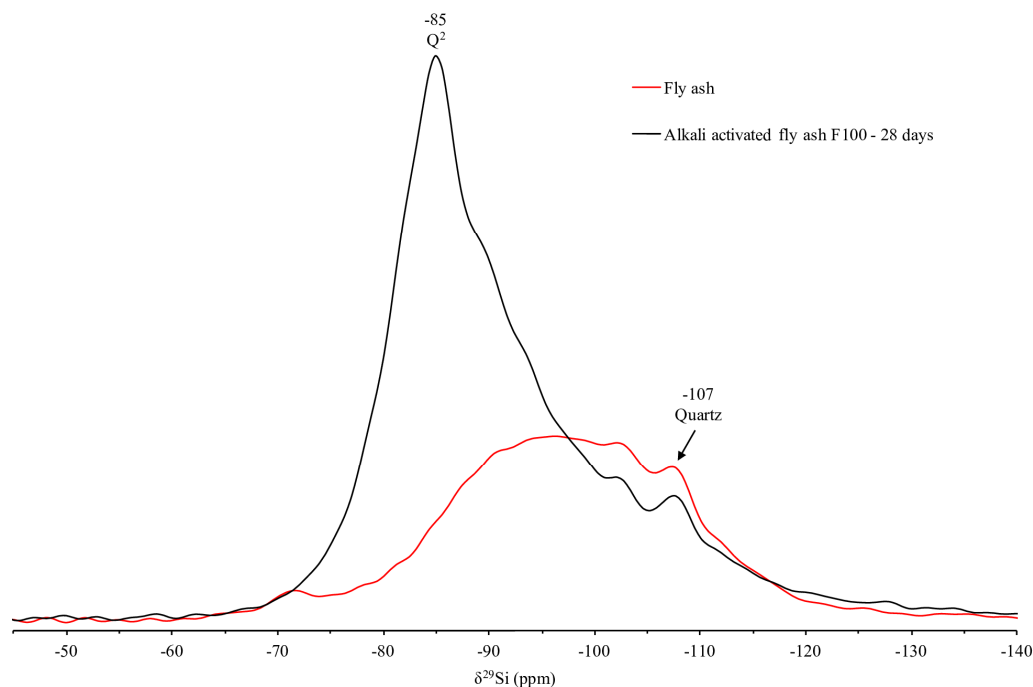
270 dissymmetrical shapes are due to electric field gradient distribution caused by the
 271 distribution of geometries of the AlO_4 and AlO_6 polyhedra.. More specifically, the
 272 main resonance whose maximum is detected at 55 ppm corresponds to Al(IV) of the
 273 vitreous phase. While the resonance located at 3 ppm corresponds to Al(VI) of the
 274 vitreous phase.



275 Fig. 6. ^{27}Al MAS-NMR spectra of the raw fly ash and alkali activated fly ash at 28 days.
 276

277 Comparatively, the high-calcium fly ash based alkali activated material spectrum at 28
 278 days exhibits a main resonance sharper and a maximum shifted to 59 ppm
 279 corresponding to four-fold coordination of aluminium namely $\text{q}^4(4\text{Si})$. Those
 280 modifications in the spectrum compared to the original high-calcium fly ash indicate
 281 that part of the aluminium released from high-calcium fly ash leads to the formation a
 282 new aluminium bearing phase whose aluminium is tetrahedrally coordinated. Lastly, the
 283 resonance owed to octahedral aluminium at 3 ppm is still present which means that
 284 high-calcium fly ash is not totally dissolved after 28 days.

285 Fig. 7 shows ^{29}Si MAS-NMR spectra of the original high-calcium fly ash as well as the
 286 alkali activated high-calcium fly ash at 28 days. ^{29}Si NMR spectrum of the original
 287 high-calcium fly ash shows a broad resonance between -85 and -105 ppm attributed to
 288 the presence of a wide range of Q^3 and Q^4 silicon local environments from the vitreous
 289 phase.



290
 291 Fig. 7. ^{29}Si MAS-NMR spectra of the raw fly ash and alkali activated fly ash at 28 days.

292 In contrast, the alkali activated high-calcium fly ash spectrum at 28 days displays a clear
 293 additional resonance centred at -85 ppm. This new position can be attributed to both the
 294 formation of $\text{Q}^4(4\text{Al})$ or else Q^2 -type silicon environments. Nevertheless, regarding the
 295 high value of the Si/Al ratio around 3.2 in the denser area comprising the new products,
 296 and measured by SEM (see Table 3) it is unlikely that $\text{Q}^4(4\text{Al})$ environments are
 297 present. The new resonance at -85 ppm consequently indicates the formation of Q^2 -type
 298 silicon environments in chain structure. Considering that the spectrum does not show
 299 any resonance corresponding to Q^1 silicon environments the length of those formed
 300 chains is high. It is also worth noting that Q^2 Si environments in chain possess a charge

301 deficit of 2- which must be compensated. However, sodium cations are not available as
302 they are associated with sulphur to form thenardite Na_2SO_4 (see sections 3.1.1 and
303 3.1.3). Consequently, only calcium cations released from calcium reactive phases of
304 high-calcium fly ash can compensate this charge deficit. Those silicon chain structures
305 are therefore combined with dissolved calcium which matches with the chemical
306 composition of the denser reactive area primarily made of silicon and calcium (see
307 Table 2). The significant broadening of the resonance at -85 ppm also indicates that
308 those chains are not well organised as C-S-H structures generally observed in Portland
309 cement [34]. Considering the low Ca content of the raw fly ash, the line broadening
310 fully agrees with amorphous C-S-H with a low Ca/Si ratio.

311 Finally, the broadest part of the activated high-calcium fly ash spectrum at 28 days from
312 -90 ppm to -100 pm indicates the presence of Q^3 and Q^4 environments mainly issued
313 from the remaining vitreous phase of high-calcium fly ash, and in accordance with the
314 previous observations of unreacted high-calcium fly ash particles at 28 days by SEM
315 (see 3.1.4.2).

316 In summary, both ^{29}Si and ^{27}Al MAS-NMR spectroscopy indicates the formation of
317 new signals following alkaline activation. It is of interest to understand whether the new
318 aluminium-containing phase seen in ^{27}Al NMR correlates with the silicate chain
319 structure observed in ^{29}Si NMR. As a comparison, aluminium in linear structure such as
320 C-S-H is either found (i) as Q^2 environments corresponding to aluminium substituting
321 for silicon atoms, and located around 68-74 ppm in ^{27}Al NMR or else (ii) as Q^3
322 environments corresponding to crosslinking through alumina bridging tetrahedra
323 positioned around 63-68 ppm in ^{27}Al NMR [35-37]. However, as mentioned above, the
324 new aluminium resonance observed in our investigation at 59 ppm would rather

correspond to $q^4(4Si)$ environment. Consequently, if aluminium is incorporated into the silicate chain structure, it would be in a three-dimensional environment which has not been described in literature yet. To conclude, results concerning the alkali activated high-calcium fly ash binder showed that calcium-rich phases constitute the reactive part of the raw high-calcium fly ash, while its vitreous phase remains mainly unreactive. The new compounds formed are mainly located around calcium-rich reactive particles and present a complex chemistry and structure which differ from cementitious compounds generally encountered in cement or lime based system.

3.2 Interaction between the alkali activated high-calcium fly ash binder and kaolin

The following section aims at understanding the interaction between kaolin and the alkali activated high-calcium fly ash binder previously described. More specifically, it aims at answering the following question: does the presence of kaolin modify the reaction sequence?

Two stabilised soils were studied i.e. KF50 for which the solid phase is made in mass of 50% of high-calcium fly ash and 50% of kaolin, and KF20 made of 20% of high-calcium fly ash and 80% of kaolin. Observations made for these two mixes turned out to be similar for all the techniques used. Therefore, only the results of KF50 will be shown while the results of KF20 can be found in Supporting Information.

Firstly, Fig. 3B shows the infrared spectrum of the original kaolin as well as the spectra belonging to the alkali activated soil KF50 as a function of time. The four bands observed in the $3695\text{--}3620\text{ cm}^{-1}$ range are typical of the presence of kaolinite, and arise from the vibration of its internal OH groups. Notably, disorder in kaolinite is mainly

349 detectable in this OH-stretching region by FTIR [38]. Those bands being still observed
350 over time in the alkali activated soils suggest that kaolinite does not react under alkaline
351 conditions. The smaller heights seen at 7 and 28 days are only due to higher sample
352 densities at higher curing times after the formation of new compounds, leading to
353 smaller probed distance and therefore lesser absorbance.

354

355 Fig. A.3 (see appendices) shows XRD patterns of the activated soil KF50 as a function
356 of curing time. Similarly to the alkali activated high-calcium fly ash binder (see 3.1.1),
357 it indicates the dissolution of anhydrite CaSO_4 along with the formation of thenardite
358 Na_2SO_4 .

359

360 Fig. 5E, F, G and H shows microstructural observations of the alkali activated kaolin
361 KF50. At 1 day, and in contrast with the alkali activated high-calcium fly ash (Fig. 5A),
362 KF50 presents a relatively low porosity due to the presence of small-sized kaolinite
363 platelets filling the pores (Fig. 5E). At 28 days, and in a similar way to the activated
364 high-calcium fly ash (Fig. 5B), KF50 presents a more compact microstructure around
365 calcium-rich phases (see encircled area in Fig. 5F).

366 Furthermore, by comparing the alkali activated high-calcium fly ash binder (Fig. 5C and
367 D) with the activated soil KF50 (Fig. 5G and H), kaolinite platelets are distinctly
368 observed (see red arrows as an example of platelet observation), and homogeneously
369 spread across the whole sample. In fact, kaolinite platelets were observed not merely in
370 the matrix but also in the most reactive massive areas supporting that kaolinite does not
371 react even in the reactive areas but rather acts as a filler.

372 Table 2 gives an average chemical composition of KF50 massive areas. It shows similar
373 tendencies than for the alkali activated high-calcium fly ash binder F100. Only slightly
374 higher contents of silicon and aluminium are measured for KF50 due to the presence of
375 kaolinite.

376 Fig. 8 shows ^{27}Al MAS-NMR spectra of the alkali activated high-calcium fly ash binder
377 F100 studied in the first section, and the alkali activated soil KF50 at 1 and 28 days. By
378 comparison with the binder F100, ^{27}Al NMR spectroscopy of KF50 displays two
379 additional resonances due to the presence of kaolin i.e. a main resonance at 4 ppm due
380 to Al(VI) of the octahedral layer of kaolinite, and a resonance at 70 ppm owed to Al(IV)
381 and corresponding to substitution of Al for Si in the tetrahedral layer of kaolinite and
382 muscovite.

383 At 1 day, KF50 presents a resonance whose maximum is located at 55 ppm and owed to
384 the vitreous phase of high-calcium fly ash, while at 28 days a shift of this resonance to
385 58 ppm indicates the formation of tetrahedral aluminium in $q^4(4\text{Si})$ environments (as
386 previously described for the alkali activated high-calcium fly ash in section 3.1.5).

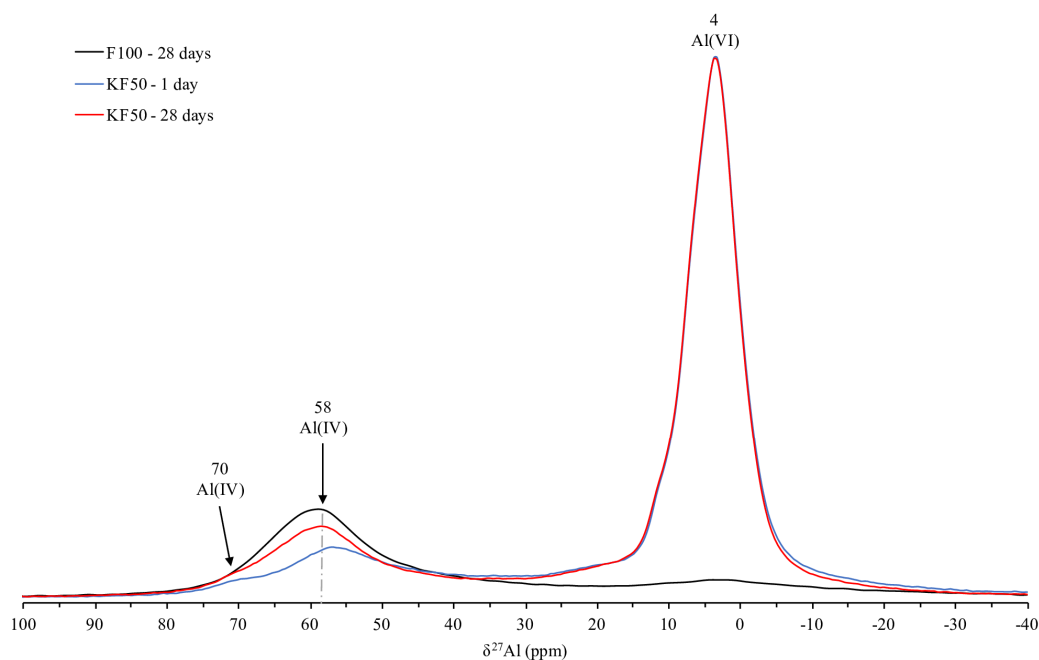


Fig. 8. ^{27}Al MAS-NMR spectra of the alkali activated fly ash F100 at 28 days and alkali activated kaolin KF50 at 1 and 28 days.

Fig. 9 shows ^{29}Si MAS-NMR spectra of the alkali activated high-calcium fly ash binder F100 studied in the first section, and the alkali activated soil KF50 at 1 and 28 days. ^{29}Si NMR spectroscopy of KF50 samples show an additional thin resonance at -91 ppm corresponding to the silicon of the tetrahedral layer of kaolinite. This resonance does not undergo any modification over time confirming the non-reactivity of kaolinite. Furthermore, from 1 to 28 days KF50 shows the clear appearance of a resonance at -85 ppm due to the formation of silicon chains combined with dissolved calcium, and as previously described for the alkali activated high-calcium fly ash binder (see 3.1.5).

To conclude, results of this second section showed that kaolin is unreactive during alkaline attack. Besides, a similar reaction sequence than for the alkali activated high-calcium fly ash binder occurs.

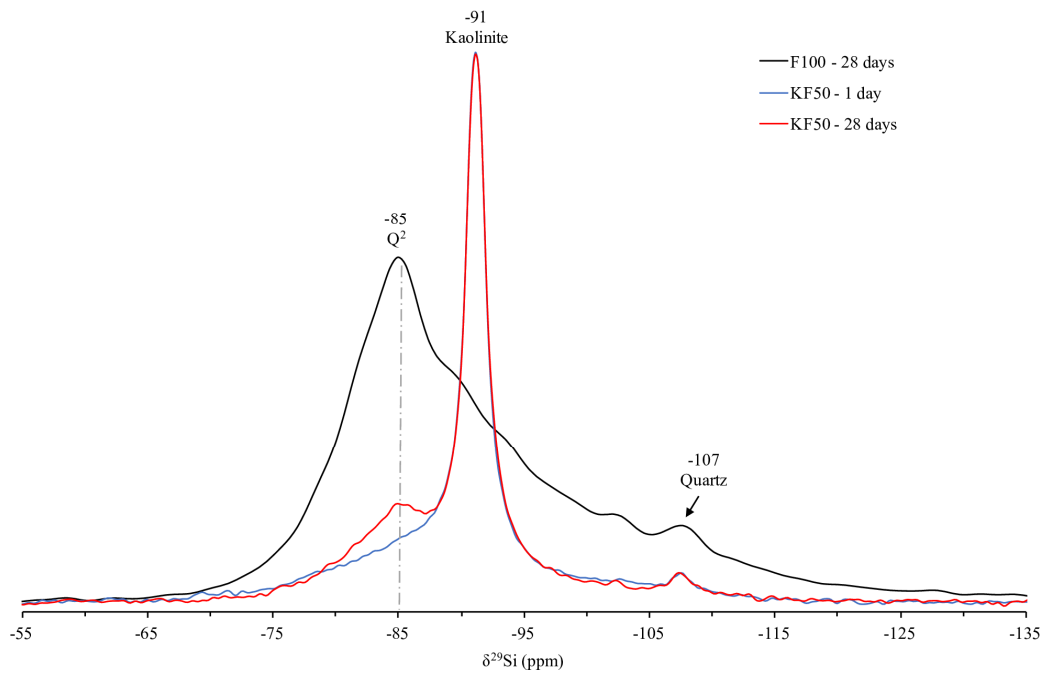


Fig. 9. ^{29}Si MAS-NMR spectra of the alkali activated fly ash F100 at 28 days and alkali activated kaolin KF50 at 1 and 28 days.

3.3 Comparison with lime treated kaolin

This last section focuses on a comparison with previous studies which reported the physicochemical evolution of the same kaolin treated either by a common stabiliser: lime [6], but also treated by a mix of lime and the high-calcium fly ash used here [39]. Table 4 gives a summary of the reaction sequences for each system highlighting strong differences. This section consequently aims at providing a better understanding of the consequences of those variable reaction sequences on the final material in terms of performance and durability.

Table 4

Compared reactivity sequences of kaolin treated either by lime, or a mix of lime and fly ash or an alkali activated fly ash

	Kaolin + Lime [6]	Kaolin + Lime + Fly ash [33]	Kaolin + Alkali activated fly ash
--	-------------------	------------------------------	-----------------------------------

1. Phases dissolved		Kaolin, lime	Kaolin, lime, fly ash	Fly ash
2. Reactivity timescale		Slow	Fast	Fast
3. Phases formed	Aluminate	Calcium Aluminate Hydrate C-A-H Monocarboaluminate hydrate C ₄ -A-C-H ₁₁	Calcium Aluminate Hydrate C-A-H Calcium Aluminium Oxide Carbonate Hydrate C-A-O-C-H Calcium Aluminium Oxide Hydrate C-A-O-H Ettringite Ca ₆ Al ₂ (SO ₄) ₃ (OH) ₁₂ .26H ₂ O	Amorphous silicate consisting of chains combined with calcium - and probably incorporating the observed q4(4Si) aluminium environments
	Silicate	None	Calcium Silicate Hydrate C-S-H	

417

418 3.3.1 Reactivity of initial phases

419 Firstly and regarding the reactivity of the phases initially present, it was found that
420 kaolin is inert in our alkali activated samples which contrasts with the two other lime
421 based systems for which kaolinite is dissolved. The limited reactivity of kaolinite in the
422 alkali activated soils herein studied is due to the presence of other more reactive phases.
423 Besides, its limited reactivity is beneficial for the system as no side effects will occur.
424 For the three systems, calcium-containing phases constitute the main reactive part of the
425 mixes playing a pivotal role in the reaction development scheme. In fact, their
426 dissolution leads to the release of dissolved calcium into the medium and hence
427 pozzolanic activity i.e. formation of new calcium cementitious compounds responsible
428 of the strength improvement. In the case of our alkali activated soils however, it is not
429 lime CaO that constitutes a supply of calcium but calcium-containing minerals from
430 high-calcium fly ash CaSO₄, CaCO₃ or Ca(OH)₂. For all calcium-source types the
431 supply of Ca²⁺ cations remains identical. What changes is the anion simultaneously
432 released from their dissolution: when high-calcium fly ash is present the dissolution of
433 its calcium-containing minerals is accompanied by the release of various anions such as

434 OH^- , SO_4^{2-} and CO_3^{2-} influencing the reaction sequence, and with potential negative
435 effects for the durability as seen later.

436 Finally, concerning the vitreous phase of high-calcium fly ash, although amorphous and
437 hence metastable it showed few reactivity leading to a preferential pozzolanic activity
438 as seen in Portland cement, rather than polymerisation reactions associated with the
439 formation of an aluminosilicate three-dimensional network characteristic of low-
440 calcium alkali activated materials and geopolymers.

441 3.3.2 *Reactivity timescale*

442 Reactions in presence of high-calcium fly ash are fast with new compounds already
443 observed at 28 days for both systems made of kaolin, lime and high-calcium fly ash [39]
444 but also kaolin and alkali activated high-calcium fly ash. Whereas, longer reactivity
445 timescale occurs for lime treated kaolin: new cementitious compounds being previewed
446 from 60 days and clearly detected only after 270 days [6].

447 For a system made of lime and kaolin its pozzolanic activity depends on the dissolution
448 of kaolinite which constitutes the only source of aluminium and silicon. Considering
449 that kaolinite possesses a stable crystalline mineral structure hard to dissolve it explains
450 the slow reactivity of that system. By contrast, high-calcium fly ash contains reactive
451 phases i.e. calcium-rich phases primarily and to a small extent its vitreous phase (for the
452 high-calcium fly ash used here) thermodynamically less stable than kaolinite and
453 therefore easier to dissolve. That is why reaction sequences are faster for both high-
454 calcium fly ash systems. It is even faster for our alkali activated soils as the alkaline
455 solution brings a mixture of ions ready available. Those fastest reaction times would
456 constitute an advantage in the case where the quickly formed products are as well stable
457 binding phases which will be discussed now.

458 3.3.3 *Stability and structure of the compounds formed*

459 In the case of formerly studied systems made of kaolin and lime as well as kaolin, lime
460 and high-calcium fly ash, a preferential release of aluminium over silicon from kaolinite
461 and/or high-calcium fly ash dissolution occurs conducting to the formation of
462 aluminium compounds primarily. In fact, for a lime treated kaolin Calcium Aluminate
463 Hydrate C–A–H and monocarboaluminate hydrate $C_4\text{--}A\text{--}C\text{--}H_{11}$ are formed [6]. In the
464 case of a kaolin treated by a mix of lime and high-calcium fly ash Calcium Aluminate
465 Hydrate C–A–H but also Calcium Aluminium Oxide Carbonate Hydrate C–A–O–C–H,
466 Calcium Aluminium Oxide Hydrate C–A–O–H and Ettringite
467 $\text{Ca}_6\text{Al}_2(\text{SO}_4)_3(\text{OH})_{12}\cdot 26\text{H}_2\text{O}$ are formed [39]. Whereas, in our alkali activated soils
468 investigated here, aluminium dissolved from the vitreous phase of high-calcium fly ash
469 was found in a three-dimensional four-fold environment ($q^4(4\text{Si})$) which strongly
470 contrasts with the six-fold environments found in the Calcium Aluminate Hydrates.
471 Regarding the formation of silicate compounds, none are formed in a system made of
472 kaolin and lime [6] because the dissolution of kaolinite is slow and starts by the release
473 of its aluminium. Hence, no silicon is made available. Kaolinite being the only source of
474 silicon in that system the limited dissolution of silicon implies the non-formation of
475 silicon compounds. By contrast in a kaolin, lime and high-calcium fly ash system, the
476 dissolution of silicon from the vitreous phase of high-calcium fly ash leads to the
477 formation of Calcium Silicate Hydrate C–S–H [39]. Finally, in the alkali activated soils
478 herein studied, the supply of silicon from the alkaline solution primarily and also from
479 the vitreous phase of high-calcium fly ash leads to the formation of silicon chains
480 combined with calcium, but whose NMR signature greatly differs from C–S–H
481 commonly observed as described above (see section 3.1.5). It is also likely that

482 aluminium found in three-dimensional four-fold environment ($q^4(4Si)$) is incorporated
483 into those silicon chains.

484 Calcium Silicate Hydrate C–S–H is the principal binding phase of Portland cement and
485 concrete primarily responsible for its strength [40]. In addition, its structure is more
486 stable than Calcium Aluminate Hydrates [41]. Their presence is consequently beneficial
487 for the performances. The fact that in our alkali activated samples, a diverse structure
488 compared to usual C–S–H is observed cannot easily be assessed in term of stability at
489 the present moment. Indeed, regarding the lack of crystallinity of our silicon chains
490 formed, experience proved that the crystallinity of the binding agent alone constitutes a
491 poor measure of stability over the timescales relevant to the majority of concrete
492 structures [41]. A further investigation of the performances would help apprehending a
493 potential beneficial effect of this uncommon silicon chains structure over time.

494

495 Finally, for both high-calcium fly ash systems, sulphate minerals are formed: either
496 Ettringite $Ca_6Al_2(SO_4)_3(OH)_{12}.26H_2O$ for a system made of kaolin, lime and high-
497 calcium fly ash [39], or Thenardite Na_2SO_4 in our alkali activated soils.

498 Their formation is due to the dissolution of anhydrite $CaSO_4$ initially present in the
499 high-calcium fly ash, and releasing sulphate anions SO_4^{2-} that are subsequently
500 recombining with available cations. For the case of a kaolin, lime and high-calcium fly
501 ash system the formation of Ettringite is taking up aluminium and calcium hence
502 slowing down both the simultaneous formation of aluminate and silicate hydrates.
503 Whereas, in our alkali activated system, sodium cations ready available from the
504 alkaline solution combine with sulphate anions. Therefore, the formation of sulphate
505 minerals does not affect the parallel development of the pozzolanic activity i.e. the

506 formation of silicate chains. Finally, a key point to consider for durability aspects is the
507 high solubility of sulphate minerals which are few stable salts in water. In fact, a
508 previous study in which leaching tests were performed on an alkali activated sulphate-
509 bearing kaolin showed that the uptake of sulphate anions by the gel is low, namely less
510 than 40% [42]. The study of the effect of wetting-drying cycles is consequently
511 warranted to verify a further impact of the presence of thenardite on the long-term
512 performances.

513 **3 Conclusions**

514 Here, the development of a novel soil binder that is an alkali activated calcium-rich
515 high-calcium fly ash for clay soil stabilisation was explored. The study of its reactivity
516 showed that (i) the overall calcium-bearing minerals from high-calcium fly ash
517 constitute the reactive phases while its vitreous phase remains mainly unreactive, (ii)
518 new compounds are formed, thenardite Na_2SO_4 and an amorphous silicate consisting of
519 chains combined with calcium - (iii) reactions happen within 1 to 28 days.

520 The interaction between the binder developed and the model soil chosen i.e. kaolin,
521 showed that kaolin is unreactive. Its presence whatever the proportion does not modify
522 the physicochemical evolution of the system that is neither the dissolved phases, formed
523 compounds, nor reactivity timescale. The inert kaolinite platelets were in addition found
524 homogenously embedded in the matrix acting as a filler.

525 When compared to lime treated kaolin, although pozzolanic activity remains the
526 dominant process reaction sequences are strongly different. In the case of alkali
527 activated soils the formation of calcium-silicon chains phases more stable than calcium
528 aluminium hydrates encountered in lime based systems is beneficial for long-term
529 stability purpose. Those observed silicon chains however show an uncommon structure

530 whose effect on the performances will be checked in a future investigation. Finally, the
 531 formation of thenardite a highly soluble salt in water raises interest about the durability
 532 of the material which will be also further investigated.

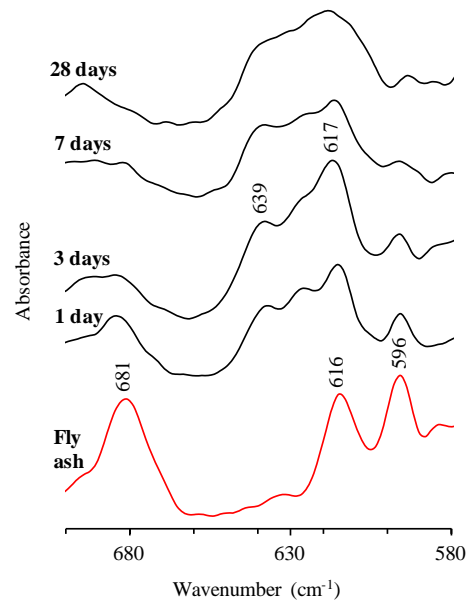
533

534 **Acknowledgements**

535 The authors wish to acknowledge the support of the European Commission via the
 536 Marie Skłodowska-Curie Innovative Training Networks (ITN-ETN) project TERRE
 537 'Training Engineers and Researchers to Rethink geotechnical Engineering for a low
 538 carbon future' (H2020-MSCA-ITN-2015-675762).

539

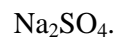
540 **Appendices**

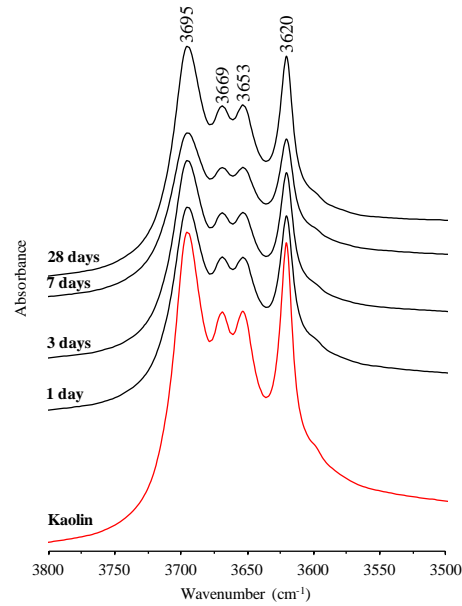


541

542 Fig. A.1. FTIR of raw high-calcium fly ash, and high-calcium fly ash based alkali
 543 activated material F100 as a function of curing time in the SO_4^{2-} stretching vibrations
 544 range; 681, 616 and 596 cm^{-1} = anhydrite CaSO_4 ; 639 and 617 cm^{-1} = thenardite

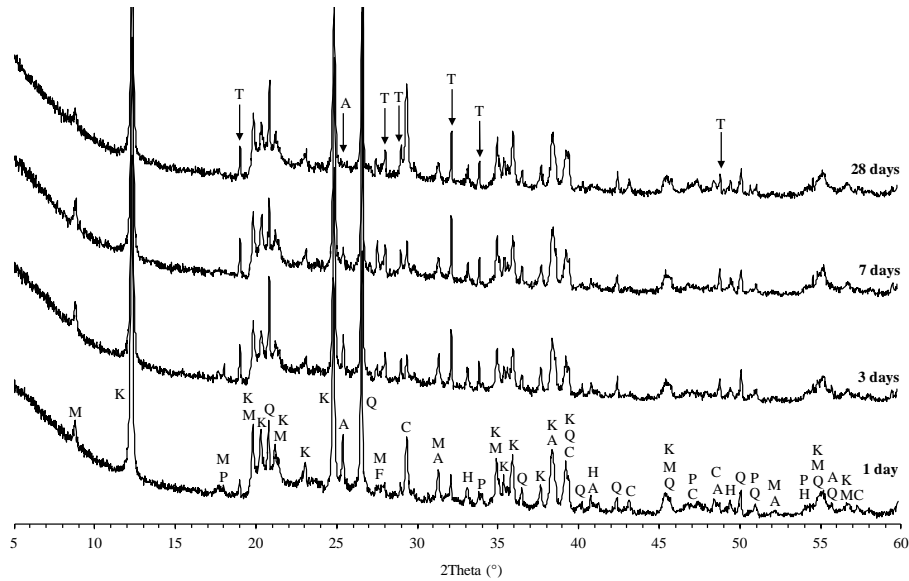
545





546

547 Fig. A.2. FTIR of the raw kaolin and alkali activated kaolin KF20 as a function of
548 curing time in the OH stretching vibrations range.



549

550 Fig. A.3. XRD of alkali activated kaolin KF50 as a function of curing time;

551 A=anhydrite; C=calcite; F=feldspar; H=hematite; K=kaolinite; M=muscovite;

552 P=portlandite; Q=quartz; T=thenardite.

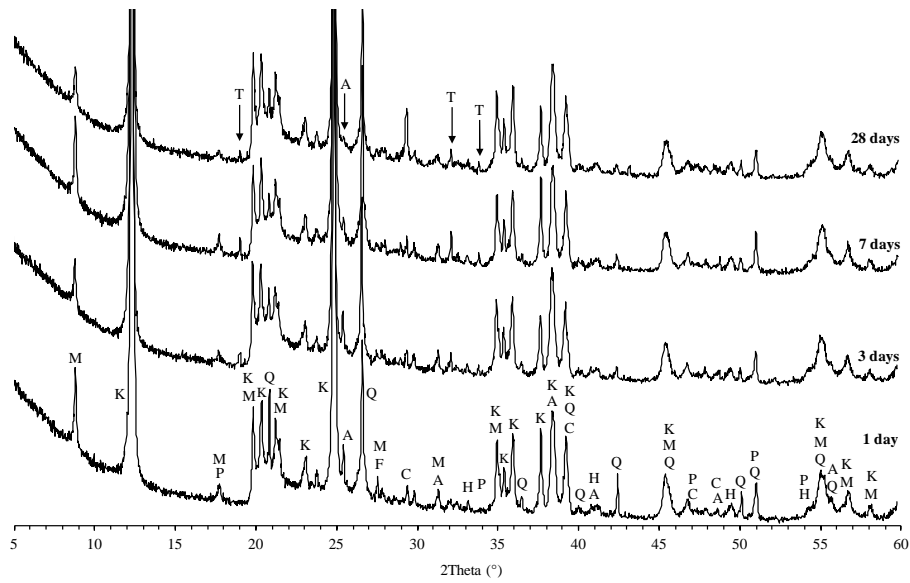


Fig. A.4. XRD of the alkali activated kaolin KF20 as a function of curing time;
A=anhydrite; C=calcite; F=feldspar; H=hematite; K=kaolinite; M=muscovite;
P=portlandite; Q=quartz; T=thenardite.

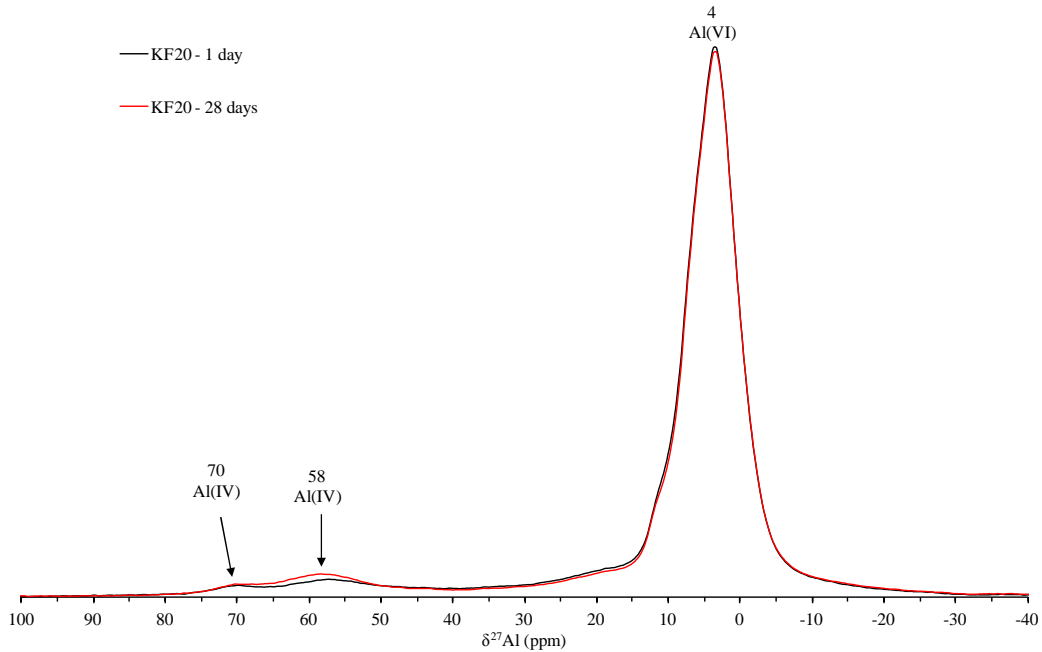


Fig. A.5. ^{27}Al MAS-NMR of the raw high-calcium fly ash, raw kaolin and alkali
activated kaolin KF20 at 0 and 28 days.

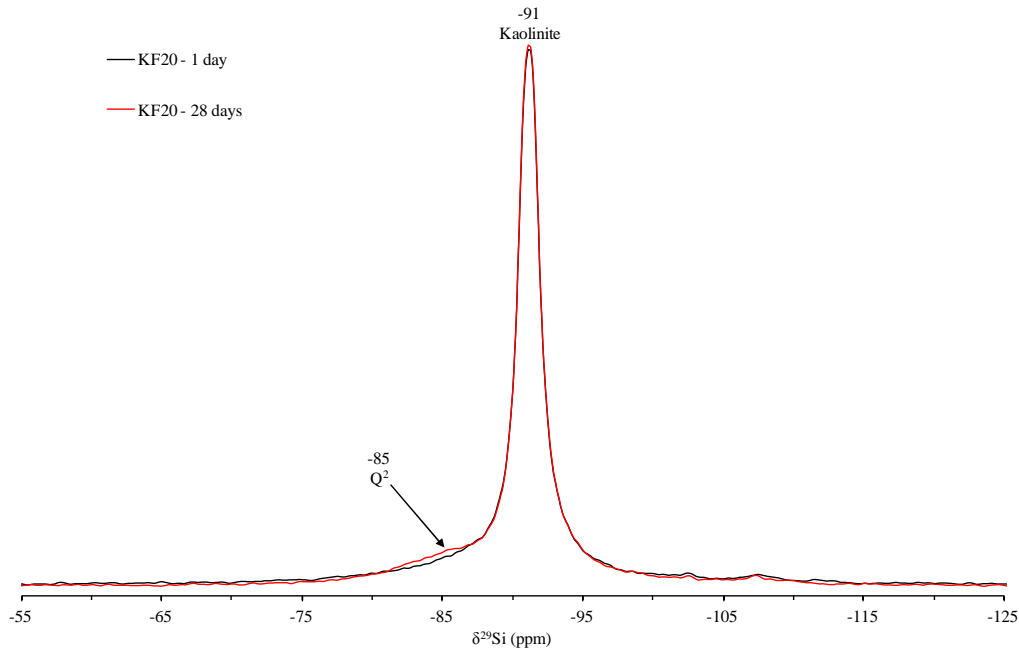


Fig. A.6. ^{29}Si MAS-NMR of the raw high-calcium fly ash, raw kaolin and alkali activated kaolin KF20 at 0 and 28 days.

References

- [1] Pomakhina, E., Deneele, D., Gaillot, A.-C., Paris, M., Ouvrard, G., 2012. ^{29}Si solid state NMR investigation of pozzolanic reaction occurring in lime-treated Ca-bentonite. *Cem. Concr. Res.* 42, 626–632.
- [2] Lemaire, K., Deneele, D., Bonnet, S., Legret, M., 2013. Effects of lime and cement treatment on the physicochemical, microstructural and mechanical characteristics of a plastic silt. *Eng. Geol.* 166, 255–261.
- [3] Chemed, Y.C., Deneele, D., Christidis, G.E., Ouvrard, G., 2015. Influence of hydrated lime on the surface properties and interaction of kaolinite particles. *Appl. Clay Sci.* 107, 1–13.
- [4] Deneele, D., Le Runigo, B., Cui, Y. J., Cuisinier, O., Ferber, V., 2016. Experimental assessment regarding leaching of lime-treated silt. *Constr. Build. Mater.* 112, 1032–1040.
- [5] Maubec, N., Deneele, D., Ouvrard, G., 2017. Influence of the clay type on the strength evolution of lime treated material. *Appl. Clay Sci.* 137, 107–114.

584
585 [6] Vitale, E., Deneele, D., Paris, M., Russo, G., 2017. Multi-scale analysis and time
586 evolution of pozzolanic activity of lime treated clays. *Appl. Clay Sci.* 141, 36–45.
587
588 [7] Guidobaldi, G., Cambi, C., Cecconi, M., Deneele, D., Paris, M., Russo, G., Vitale,
589 E., 2017. Multi-scale analysis of the mechanical improvement induced by lime addition
590 on a pyroclastic soil. *Eng. Geol.* 221, 193–201.
591
592 [8] Scrivener, K.L., Kirkpatrick, R.J., 2008. Innovation in use and research on
593 cementitious material. *Cem. Concr. Res.* 38, 128–136.
594
595 [9] Rahman, A., 1986. The Potentials of Some Stabilizers for the Use of Lateritic Soil in
596 Construction. *Build. Environ.* 21, 57–61.
597
598 [10] Basha, E.A., Hashim, R., Muntohar, A., 2003. Effect of the cement-rice husk ash
599 on the plasticity and compaction of soil. *Electron. J. Geotech. Eng.* 8.
600
601 [11] Nalbantoğlu, Z., 2004. Effectiveness of Class C fly ash as an expansive soil
602 stabilizer. *Constr. Build. Mater.* 18, 377–381.
603
604 [12] Koliass, S., Kasselouri-Rigopoulou, V., Karahalios, A., 2005. Stabilisation of clayey
605 soils with high calcium fly ash and cement. *Cem. Concr. Compos.* 27, 301–313.
606
607 [13] Parsons, R.L., Kneebone, E., 2005. Field performance of fly ash stabilised
608 subgrades. *Ground Improv.* 9, 33–38.
609
610 [14] Sharma, U., Khatri, A., Kanoungoc, A., 2014. Use of Micro-silica as Additive to
611 Concrete-state of Art. *Int. J. Civ. Eng. Res.* 5, 9–12.
612
613 [15] James, J., Pandian, P.K., 2016. Industrial Wastes as Auxiliary Additives to
614 Cement/Lime Stabilization of Soils. *Adv. Civ. Eng.* 2016, 1–17.
615
616 [16] Singhi, B., Laskar, A.I., Ahmed, M.A., 2016. Investigation on Soil–Geopolymer
617 with Slag, Fly Ash and Their Blending. *Arab. J. Sci. Eng.* 41, 393–400.
618
619 [17] Wilkinson, A., Haque, A., Kodikara, J., 2010. Stabilisation of clayey soils with
620 industrial by-products: part A. *Proc. Inst. Civ. Eng. - Ground Improv.* 163, 149–163.
621
622 [18] Cristelo, N., Glendinning, S., Teixeira Pinto, A., 2011. Deep soft soil improvement
623 by alkaline activation. *Proc. Inst. Civ. Eng. - Ground Improv.* 164, 73–82.
624
625 [19] Phummiphan, I., Horpibulsuk, S., Rachan, R., Arulrajah, A., Shen, S-L.,
626 Chindaprasirt, P. 2018. High Calcium Fly Ash Geopolymer Stabilized Lateritic Soil and
627 Granulated Blast Furnace Slag Blends as a Pavement Base Material, *Journal of*
628 *Hazardous Materials*, *Journal of Hazardous Materials*, 341, pp. 257-267
629 [20] Cristelo, N., Glendinning, S., Fernandes, L., Pinto, A.T., 2012. Effect of calcium
630 content on soil stabilisation with alkaline activation. *Constr. Build. Mater.* 29, 167–174.
631

632 [21] Rios, S., Cristelo, N., Viana da Fonseca, A., Ferreira, C., 2016. Structural
633 Performance of Alkali-Activated Soil Ash versus Soil Cement. *J. Mater. Civ. Eng.* 28,
634 4015125.
635

636 [22] Tenn, N., Allou, F., Petit, C., Absi, J., Rossignol, S., 2015. Formulation of new
637 materials based on geopolymer binders and different road aggregates. *Ceram. Int.* 41,
638 5812–5820.
639

640 [23] Sargent, P., Hughes, P.N., Rouainia, M., White, M.L., 2013. The use of alkali
641 activated waste binders in enhancing the mechanical properties and durability of soft
642 alluvial soils. *Eng. Geol.* 152, 96–108.
643

644 [24] Zhang, M., Guo, H., El-Korchi, T., Zhang, G., Tao, M., 2013. Experimental
645 feasibility study of geopolymer as the next-generation soil stabilizer. *Constr. Build.*
646 *Mater.* 47, 1468–1478.
647

648 [25] Silva, R.A., Oliveira, D.V., Miranda, T., Cristelo, N., Escobar, M.C., Soares, E.,
649 2013. Rammed earth construction with granitic residual soils: The case study of
650 northern Portugal. *Constr. Build. Mater.* 47, 181–191.
651

652 [26] Buchwald, A., Kaps, C., Hohmann, M., 2003. Alkali-activated binders and
653 pozzolan cement binders—complete binder reaction or two sides of the same story, in:
654 Proceedings of the 11th International Conference on the Chemistry of Cement. Portland
655 Cement Association Durban, South Africa, pp. 1238–1246.
656

657 [27] Shi, C., Krivenko, P.V., Roy, D.M., 2006. Alkali-activated cements and concretes.
658 Taylor & Francis, London ; New York.
659

660 [28] Sukmak, P., Horpibulsuk, S., Shen, S-L., Chindaprasirt, P., Suksiripattanapong, C.
661 2013. Factors influencing strength development in clay-fly ash geopolymer, *Constr.*
662 *Build. Mater.*, 47, 1125-1136.
663

664 [29] Sukmak, P., De Silva, P., Horpibulsuk, S., Chindaprasirt, P. 2015. Sulphate
665 resistance of clay-Portland cement and clay-high calcium fly ash geopolymer, *J. Mater.*
666 *Civ. Eng.*, Vol. 27, No. 5, 04014158.
667 [30] Snellings, R., Mertens, G., Elsen, J., 2012. Supplementary Cementitious Materials.
668 *Rev. Mineral. Geochem.* 74, 211–278.
669

670 [31] Newman, E.S. 1941. Behaviour of calcium sulfate at high temperatures. *J. of Res.*
671 *of Nat. Bur. of Stand.*, Vol 27, 191-196.
672

673 [32] Stern, K. H., and Weise, E. L. 1966. High temperature properties and
674 decomposition of Inorganic salts – Part 1 – Sulfates. National Standard Reference Data
675 Series- National Bureau of Standards 7, Issued October 1, 52p.
676

677 [33] Pop S-F., Ion, R.M. 2013. Thermal analysis of the chemical weathering of chalk
678 stone materials. *J. of Optoelect. And Adv. Mat.*, Vol 15, No. 7- 8, 888 – 892.

679 [34] Cong, X., Kirkpatrick, R.J., 1996. ^{29}Si MAS NMR study of the structure of
680 calcium silicate hydrate. *Adv. Cem. Based Mater.* 3, 144–156.
681

682 [35] Andersen, M.D., Jakobsen, H.J., Skibsted, J., 2003. Incorporation of Aluminum in
683 Calcium Silicate Hydrate (C–S–H) of Hydrated Portland Cements: A High-Field ^{27}Al
684 and ^{29}Si MAS NMR Investigation. *Inorg. Chem.* 42, 2280–2287.
685

686 [36] Sun, G.K., Young, J.F., Kirkpatrick, R.J., 2006. The role of Al in C–S–H: NMR,
687 XRD, and compositional results for precipitated samples. *Cem. Concr. Res.* 36, 18–29.
688

689 [37] Pardal, X., Brunet, F., Charpentier, T., Pochard, I., Nonat, A., 2012. ^{27}Al and ^{29}Si
690 Solid-State NMR Characterization of Calcium-Aluminosilicate-Hydrate. *Inorg. Chem.*
691 51, 1827–1836.
692

693 [38] Wilson M.J., 1994. *Clay mineralogy: spectroscopic and chemical determinative*
694 *methods*, Springer Science + Business Media.
695

696 [39] Knapik K, 2016. Experimental and numerical analyses of fly ash from fluidized
697 bed combustion applications for selected ground improvement. The Silesian University
698 of Technology, PhD thesis, 217p.
699

700 [40] Tajuelo Rodriguez, E., Garbev, K., Merz, 650 D., Black, L., Richardson, I.G.,
701 2017. Thermal stability of C-S-H phases and applicability of Richardson and Groves’
702 and Richardson C-(A)-S-H(I) models to synthetic C-S-H. *Cem. Concr. Res.* 93, 45–56.
703

704 [41] Provis John L., van Deventer Jannie S.J., 2009. *Geopolymers Structure,*
705 *processing, properties and industrial applications*, Woodhead Publishing in materials.
706 Woodhead, Cambridge.
707

708 [42] Occhipinti R., Tarantino S. C., Riccardi M. P., Sturini M., Speltini A., Maraschi F.,
709 Elmaleh A., Zema M., 2017. Alkali activation of sulfate-bearing kaolin. *Proceedings of*
710 *the 16th International Clay Conference*, Granada, Spain.
711